Ultra-Low-loss Reconfigurable Phase-shifting Metasurface in V band: A Multi-objective Optimization Approach

Pablo H. Zapata Cano, *Student Member, IEEE,* Evangelos Vassos, Zaharias D. Zaharis, *Senior Member, IEEE,* Pavlos I. Lazaridis, *Senior Member, IEEE,* Traianos V. Yioultsis, *Member, IEEE,* Nikolaos V. Kantartzis, *Senior Member, IEEE,* and Alexandros P. Feresidis, *Senior Member, IEEE*

***Abstract*—Future generations of satellite and mobile communications at mm-wave frequencies require the use of low-loss and wideband phase-shifting components. Pixelated metasurfaces provide large design versatility and constitute an attractive solution for wave manipulation, such as shifting the phase of an incident wave. However, their design often implies the simultaneous tuning of a large number of geometrical parameters. This article employs an enhanced multi-objective optimization algorithm to design a dynamically reconfigurable metasurface providing ultra-low losses and linear phase response. The presented methodology can be easily employed for different objective functions or technologies, constituting a versatile design strategy for electromechanically reconfigurable devices based on pixelated metasurfaces. A prototype is fabricated based on the optimization outcome, achieving a phase shifter capable of providing a continuous phase shift up to 180° between 50 and 65 GHz. A piezo-electric actuator is used to dynamically adjust the phase shift with respect to the position of a metallic ground plane placed in front of the metasurface. A linear evolution of the phase w.r.t. the ground plane displacement is obtained while maintaining the losses around 1 dB for the whole frequency range.**

***Index Terms*—Phase shifter, millimeter wave, pixel metasurface, optimization, piezoelectric actuator, wave manipulation.**

I. Introduction

Phase shifting is considered one of the most crucial functionalities in microwave components. Phase shifters play a key role in many antenna designs such as reflectarray antennas [1], transmittarrays [2], and phased arrays [3], but are also crucial in other mm-wave and THz components and applications like absorbers [4], propagating mode to surface mode conversion [5], or anisotropic polarization converters [6].

Existing technologies for the design of reconfigurable phase shifters for antenna applications include diode phase shifters [7], ferrite phase shifters [8] or multiport-differential phase shifters [9]. However, these methods often involve complex circuitry or the necessity of switching elements [10], and they often suffer from high losses. Thus, the exploration of alternative low-loss reconfiguration mechanisms has been a research topic of interest recently. The utilization of metasurfaces consisting of an ordered metallic geometry patterned onto a dielectric substrate contributes to simultaneous control of the magnitude, phase, and polarization of electromagnetic waves [11], [12]. In order to conceive reconfigurable unit cells, solutions involving the utilization of varactors and/or PIN diodes have been widely used to achieve spatial manipulation of the electromagnetic fields [13], [14], [15]. Unfortunately, these devices suffer from high losses and large packaging volumes at high frequencies. The aforementioned issues motivate the utilization of other reconfiguration strategies like electromechanical systems, in which the reconfiguration engine is placed outside the metasurface, hence not introducing any extra loss. In this context, a novel technique for tuning periodic phase-shifting metasurfaces at high mm-wave frequencies was presented in [16]. This was exploited in [17] to design a low-loss tunable phase shifter achieving up to 360° by means of a piezo-electric actuator.

The choice of the most suitable lattice for the unit cell in such designs is a complex problem with a very wide range of possibilities. In most of the works mentioned previously, relatively simple unit cell designs were adopted, and only a few geometrical parameters were considered throughout the design process. Through advanced optimization techniques, innovative unit cell geometries that are not necessarily intuitive at first sight can be reached [18]. Optimization-driven design using nature-inspired techniques like genetic algorithms (GAs) or particle swarm optimization (PSO) have been widely employed for the design of phased array antennas [19], frequency selective surfaces [20], and microwave absorbers [21], among others. However, these optimization techniques are mostly employed on their canonical versions, without modifying the optimization procedure to improve the algorithm's performance in the addressed problem.

Moreover, the linearity of the phase response and the loss have not been incorporated as objectives when designing the unit cell, as the main focus has been the maximum (or desired) achievable phase shift. In a previous work, optimization was employed to design a 90° phase shifter at 60 GHz [22]. A pixelated metasurface was adopted, abandoning the idea of a pre-fixed geometry for a unit cell. Moreover, the structure was designed for an optimum phase shift and minimum loss,

This research was supported by the European Union, through the Horizon 2020 Marie Skłodowska-Curie Innovative Training Networks Programme "Mobility and Training for beyond 5G Ecosystems (MOTOR5G)" under grant agreement no. 861219.

P. H. Zapata (pablozapata@auth.gr), Z.D. Zaharis, T.V. Yioultsis, and N.V. Kantartzis are with the School of Electrical and Computer Engineering, Aristotle University of Thessaloniki, Thessaloniki 54124, Greece.

P. Lazaridis is with the School of Computing and Engineering, University of Huddersfield, Huddersfield HD1 3DH, U.K.

E. Vassos and A.P. Feresidis are with the Department of Electrical, Electronic and Systems Engineering, University of Birmingham, Birmingham B15 2SA, U.K.

jointly. However, only a unique phase shift was achievable since no reconfiguration system was adopted.

This work uses a multi-objective GA to design a wide-band reconfigurable phase shifter consisting of a pixelated metasurface and a mechanical actuator. A novel formulation is proposed for this problem, allowing to consider the linearity of the obtained phase response within the optimization, while minimizing the losses and obtaining a maximum desired phase shift of 180°. Due to the nature of the optimization problem, the design of the pixelated metasurface changes on every iteration of the algorithm, which signifies an extra degree of complexity compared to a simple parameter-tuning problem. This constitutes a nondeterministic polynomial (NP)-complete problem that is addressed by the joint utilization of an optimization framework implemented in Python and full-wave electromagnetic simulation, conducted using the CST Microwave Studio [23] software. Furthermore, the optimization method is enhanced by introducing a loss penalization coefficient, which aims to ensure the production of low-loss solutions without increasing the optimization complexity (i.e. adding another optimization objective function for the losses). This results in a complete design methodology for electromechanically reconfigurable devices including pixelated metasurfaces, that can easily be extended to other scenarios including more complex (non-linear) target phase distribution functions or other objectives that might include polarization and/or wide-angle response. Moreover, conclusions about the fabrication and characterization procedures are mentioned in the manuscript, including a comparison between two dielectrics with different metal layer coating. The fabricated devices are characterized, showing ultra-low losses and a good phase-shifting performance through a wide frequency range, between 50 and 65 GHz.

The rest of the paper is organized as follows: First, the design and working principle of the device are introduced in Section II. Second, the formulation of the optimization problem and the employed methodology are described in Section III, and the results obtained from optimization are presented. Next, the fabricated prototype, including the manufacturing and characterization details is presented in Section IV. The experimental results are presented and discussed in Section V. Finally, the last section contains some concluding remarks.

II. Phase Shifting Mechanism

In order to better emphasize the role of the pixelated metasurface in the phase shifting structure, the case of a simpler phase shifter without the presence of a periodic surface is introduced first. A schematic of this trivial phase shifter is included within Fig. 1, and its phase response can be easily analytically calculated by applying basic transmission line theory. In particular, the reflection coefficient of the wave after penetrating the structure and being reflected can be expressed as

$$\Gamma = \frac{Z_{in} - \eta_0}{Z_{in} + \eta_0} \tag{1}$$

where η_0 corresponds to the free space impedance and Z_{in} represents the input impedance at the upper surface of the device, modeled as

$$Z_{in} = Z_{sub}\frac{Z_{cav} + Z_{sub} \cdot \tanh(w \cdot \gamma_{sub})}{Z_{sub} + Z_{cav} \cdot \tanh(w \cdot \gamma_{sub})} \tag{2}$$

where γ_{sub} and γ_{cav} are propagation constants and $Z_{sub} = \eta_0\sqrt{1/\varepsilon_r}$ and $Z_{cav} = \eta_0 \tanh(d \cdot \gamma_{cav})$ state for the characteristic impedance of the substrate and the air cavity, respectively. The substrate is made of a dielectric material with ε_r = 2.2, a thickness of 0.78mm, and a loss tangent of 0.0009.

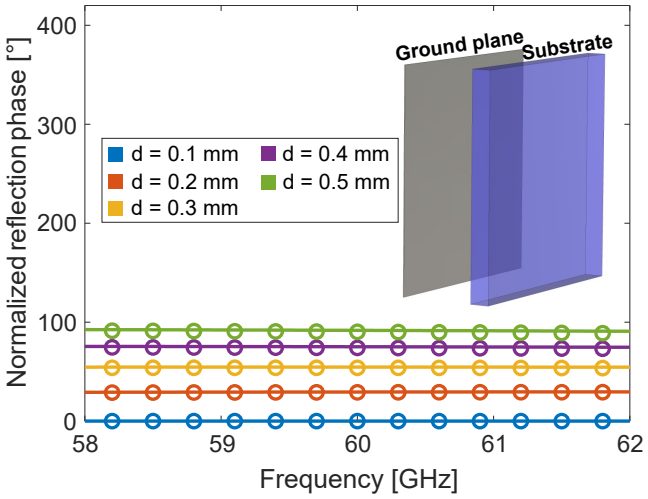

Fig. 1. Phase response of the proposed device without the presence of the periodic surface for different displacements of the ground plane. The solid lines represent the analytical results, while the circle markers correspond to the simulated result obtained via CST Microwave Studio. The case of a displacement of d = 0.1 mm is the reference chosen for normalization.

The reflection phase induced by different displacements of the ground plane, ranging from 0.1 to 0.5 mm, is shown in Fig. 1. It can be observed how a phase shift of around 90° is achieved for the maximum displacement (d = 0.5 mm).

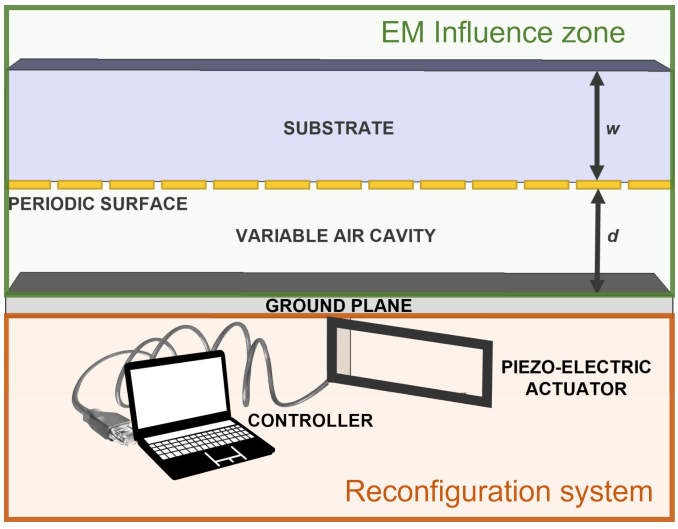

Fig. 2. Schematic of the proposed tunable phase shifter.

A periodic surface deposited on the substrate, as depicted in Fig. 2, is introduced into the design, with the aim of controlling

the induced phase shift in a smart way, while keeping the losses as low as possible and conserving a linear evolution of the phase w.r.t. the ground plane displacement.

This surface contains a periodic array of subwavelength metallic elements configured on a pixelated grid. The realization of an optimal design of this grid to satisfy the imposed requirements in terms of induced phase shift, losses, and linearity, configures the optimization problem that is addressed below.

As can be observed in Fig. 2, the metallic ground plane serves as a division between the *EM influence zone* and *reconfiguration system*, encapsulated into the green and red boxes in the image, respectively. This distinction is one of the keys to understanding the reconfiguration system's ultra-low-loss nature. In fact, the incident (and later reflected) electromagnetic wave does not penetrate the ground plane, thus never interacting with any of the elements composing the reconfiguration system. This leads to a reduction of the losses compared to other reconfiguration schemes, such as the case of active components like diodes or varactors. Furthermore, this unconventional configuration allows for accurate simulation of the entire structure without needing to include any of the devices from the reconfiguration system in the model.

III. Optimization

This section introduces the details regarding the presented optimization problem, including its formulation, implementation, and achieved results.

A. Formulation of the optimization problem

Let $\mathcal{G}$ be the set of N pixels forming the grid constituting one unit cell of the metasurface. In order to ensure the polarization invariability of the solution, vertical, horizontal, and diagonal symmetries need to be respected in the unit cell, as depicted in Fig. 3.

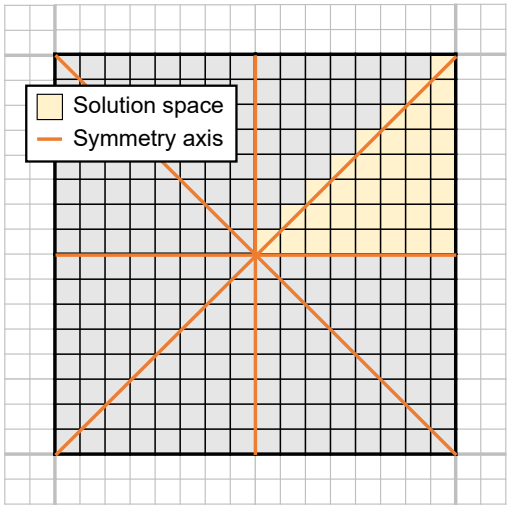

Fig. 3. Schematic of a unit cell of the metasurface, including the symmetry axes and the solution space considered for the definition of the optimization space.

Thus, considering a squared grid as a unit cell, the set of pixels composing the solution of the optimization problem reduces to $|\mathcal{P}| = \sqrt{N}(\sqrt{N}/2+1)/4$. This comprehends the pixels contained in one eighth of a unit cell, including the diagonal elements.

Then, the solution of the addressed optimization problem will be a binary array of the form $p \in \{0,1\}^{|\mathcal{P}|}$, where p_i corresponds to the state of each pixel. If the ith pixel is chosen to be metalized, then p_i is set to 1, being equal to 0 for non-metalized pixels.

By applying the symmetry rules depicted in Fig. 3, the periodic surface is constructed from the optimization solution, integrated within the rest of the components of the device, and imported to CST Microwave Studio for full electromagnetic simulation. In order to evaluate not only the maximum achieved phase shift, but also study the linearity of the induced phase shift w.r.t. the ground plane displacement, three simulations are performed every time a solution is evaluated: A first one in which the position of the metallic plate is the closest possible to the periodic surface (i.e. minimum displacement, with $d = d_1 = d_{min}$), a second in which the metallic plate is displaced to the half of the maximum displacement ($d = d_2 = d_{max}/2$), and a third one in which the displacement is set to the maximum ($d = d_3 = d_{max}$). Both the magnitude (mag_{d1}, mag_{d2}, mag_{d3}) and phase (ph_{d1}, ph_{d2}, ph_{d3}) of the reflected wave is computed for each of the three simulations. Based on that, the induced phase shifts at each of the two displaced positions of the metal plate can be calculated as $ps_{12} = |ph_{d2} - ph_{d1}|$ and $ps_{23} = |ph_{d3} - ph_{d2}|$, respectively.

The first objective of the optimization problem is related to the maximum phase shift achievable by the device (hence, for a metallic plate displacement of $d = d_{max}$). Thus, for a desirable phase shift ps_{goal} at the position of maximum displacement of the ground plane, the correspondent objective function to be minimized can be expressed as:

$$\min q_{ps} = \sum_{j=f_{min}}^{F} \left[ps_{goal} - (ps_{12} + ps_{23})\right]^2 \tag{3}$$

where $F = [f_{min}, f_{max}]$ corresponds to the frequency bandwidth of the simulation. The quadratic nature of the objective function intends to avoid the presence of abrupt phase picks (caused by some resonant behavior, often very narrow-band) by increasing their contribution to a larger (i.e. less performing) value of q_{ps}.

The second objective consists of the achievement of a linear evolution of the induced phase shift with respect to the displacement of the metal plane d. Therefore, the problem is divided into two regions: 1) corresponding to the phase shift when the metal plate is displaced from d_1 to d_2 (or d_{min} to $(d_{max} - d_{min})/2$), and 2) formed by the displacement of the ground plane from d_2 to d_3 (or $(d_{max} - d_{min})/2$ to d_{max}). Then, the second objective function is formulated as

$$\min q_{lin} = \sum_{j=f_{min}}^{F} \left|ps_{12} - ps_{goal}/2\right|^2 + \left|ps_{23} - ps_{goal}/2\right|^2 \tag{4}$$

For the presented scenario, in which we target a linear phase distribution, 2 points would be enough to perfectly depict the desired behavior of the induced phase shift vs the ground plane displacement, which is a straight line from 0° (at the initial position of the ground plane) and 180° (at the maximum ground plane displacement). However, we have observed that, if only two evaluation points are considered (i.e. a single displacement region), there is a tendency of the algorithm to provide solutions in which most part of the induced phase shift is concentrated on the initial region of the displacement (d between 0.1 and 0.3 mm). This is the reason why a third evaluation point was incorporated into the evaluation, resulting in the objective function defined in Equation 4, which considers two different displacement regions. This paradigm would not be applicable to other kinds of (non-linear, more complex) target phase shift distributions, in which more evaluation points (i.e. more displacement regions) might need to be added to better fit the target phase distribution function.

By the joint optimization of both objective functions, the problem will consist of the search for the configuration of the pixel grid that provides both a flat reflection phase (of a given target value), and a linear relation between the phase shift and the ground plane displacement. However, up until now, no considerations have been taken regarding the magnitude response of the solutions, i.e., the losses induced by the phase shifter.

In order to force the algorithm to produce low-loss solutions without increasing the complexity of the optimization problem, a penalization coefficient is added to both objective functions. If we consider l_t (in dB) to be an acceptable level of losses, and mag_{12} (mag_{23}) to be the losses induced within the first (second) displacement of the ground plane, the losses penalization coefficient α_l is defined as

$$\alpha_l = \begin{cases} 0 & \text{if } |mag_{12}| < l_t \\ |mag_{12}| & \text{otherwise} \end{cases} \tag{5}$$

for the first displacement region (an analogous expression can be easily obtained for the second region). Note that the calculation of α_l is performed for every evaluated frequency point, and the cumulative sum of all of them is then added to the two objective functions, resulting in the following final formulations: $q_{ps} = q_{ps} + \alpha_l$ and $q_{lin} = q_{lin} + \alpha_l$. With the introduction of the penalization coefficient, the losses are taken into account within the optimization method, without adding a third objective to the optimization, which would increase the complexity of the problem, thus complicating the convergence and augmenting the experimentation time. The same strategy (i.e. the modification of the objective functions with the addition of a penalization coefficient to incorporate an extra requirement without increasing the number of optimization objectives) could be applied in other scenarios, allowing to incorporate other characteristics such as the polarization invariance or the wide-angle response into the optimization scheme.

B. Optimization framework and methodology

The working of the employed optimization framework is synthesized in Fig. 4. Due to the nature of the problem, the number and position of some elements of the designs are different for every possible solution (i.e. every solution represents a different configuration of the pixel grid). Thus, such an optimization is more complex than a parameter-tuning problem and cannot be addressed with the built-in optimization tools available within most full-wave simulators. In the same way, such tools only implement canonical versions of a very restricted set of algorithms, making it impossible to modify them to perform better for particular problems. In the proposed framework, full-wave electromagnetic simulation carried on in CST Microwave Studio is integrated within an optimization engine implemented in Python, which is based on the jmetalPy platform [24].

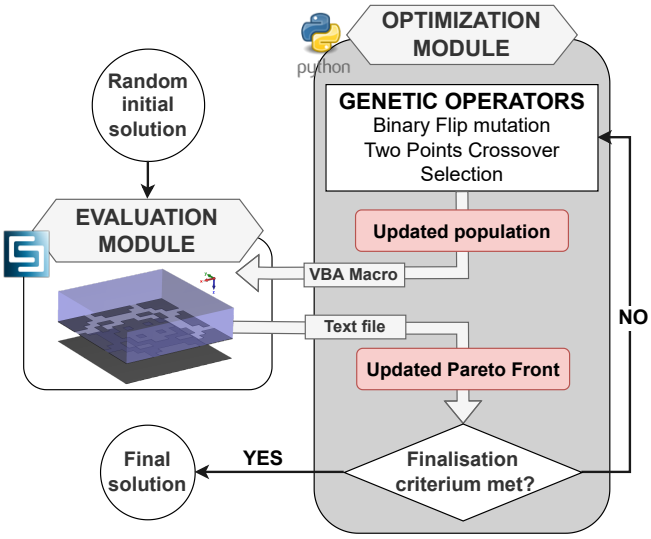

Fig. 4. Flowchart of the optimization procedure.

The algorithm used for optimization is the Non-Dominated Sorting Genetic Algorithm II (NSGA-II) [25]. It is an evolutionary technique that consists of generating new populations from the original one by applying genetic operators (selection, crossover, and mutation). Then, the individuals of both the new and the old population are evaluated and sorted out according to the value(s) of the fitness function(s). After this step, a new population is formed with the best solutions. The selected genetic operators are Bit Flip Mutation, Simplex (SPX) Crossover, and Binary Tournament Selection. The multi-objective, binary nature of the problem determines the choice of the algorithm. The NSGA-II has shown to be the most popular metaheuristic for solving multi-objective optimization problems, even for a large number of variables [26].

The metasurface that conforms the solution of the optimization problem is composed of a squared pixel grid of $N = 256$ elements. This results in $|\mathcal{P}| = 36$ variables, after applying the symmetries depicted in Fig. 3. The choice of the dimension of the unit cell is mainly determined by the application and the manufacturing limitations. In our case,

we faced the constraint of having a minimum pixel width of p_w = 0.1875 mm. Then, considering that we target normal incidence applications, a unit cell of 3x3 mm (0.6λ at 60 GHz) was adopted to both avoid the propagation of high-order Floquet modes at normal incidence and keep a grid of 256 elements, which provides enough degrees of freedom to the optimization algorithm. A maximum of 3000 evaluations has been chosen as the finalization criterion for the algorithm, and the population size is set to 20 individuals. Thus, the first population is obtained by the random generation of 20 initial solutions. The crossover and mutation operators are applied with a probability of r_c = 0.9 and $r_m = 1/|\mathcal{P}|$ = 0.0278, respectively. Regarding the optimization objectives, a maximum phase shift ps_{goal} of 180° is desired for a maximum ground plane displacement of 0.4 mm. The minimum and maximum positions of the ground plane are d_{min} = 0.1 mm and d_{max} = 0.5 mm, respectively. A threshold value of l_t = 0.5 dB is adopted for the losses penalization coefficient. Finally, the targeted operation frequency for the phase shifter is 60 GHz, which constitutes one of the devised mm-wave frequency bands for future communication systems [27]. A bandwidth of 4 GHz around the central frequency has been considered for optimization.

C. Optimization results

Fig. 5 includes the Pareto front (set of non-dominated solutions plotted in the objective space) at different stages of the optimization. Note that the values of the objective functions are averaged by frequency point. It can be appreciated how the algorithm advances significantly during the first 2000 evaluations, especially in the central part of the front. After 3000 evaluations, an acceptable level of convergence is reached and the resulting front is taken as a final solution set.

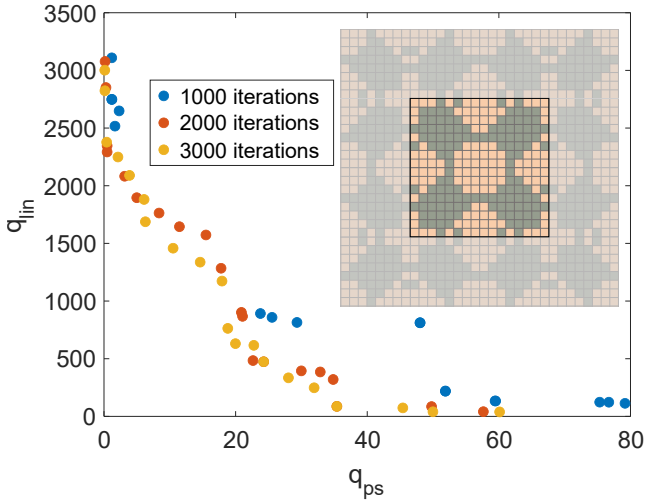

Fig. 5. Pareto front at different stages of the optimization process and geometry of the selected solution. The center box contains a single unit cell.

Also, it can be concluded from the figure that the objective related to the maximum induced phase shift q_{ps} was easier to satisfy than the one associated with the linearity q_{lin}. This is not a surprise, since even larger phase shifts achieved by similar structures have been reported in previous works [17]. However, obtaining a linear evolution of the phase w.r.t. the ground plane displacement is a very challenging task, that was not explicitly addressed before.

In order to select the most convenient solution from all the ones comprising the final Pareto front, the following strategy is adopted: First, a threshold value is selected for the maximum phase objective q_{ph}. This threshold corresponds to the maximum acceptable deviation from the desired phase shift ph_{goal} for a satisfactory performance of the device. The solutions satisfying this condition will form a sub-group of the Pareto front, conformed by solutions that satisfy the imposed requirement in terms of phase shift. Then, the most linear solution within this group is selected as the most convenient solution.

A maximum tolerable deviation of 4° is established as a threshold. This restricts the selectable solution set to the ones presenting a q_{ph} value lower than 16. The above is satisfied by a considerable number of solutions. Among them, the solution with the better q_{lin} value is selected, resulting in the final unit cell geometry, depicted in Fig. 5. The metalized pixels are represented with a clear orange color, whereas the darker gray color represents the substrate. The geometry is composed of four metallic elements: a cross, a pseudo square, and two rhombuses with rectangular gaps along the x- or y-axis. The corner of the unit cell coincides with the center of the cross element.

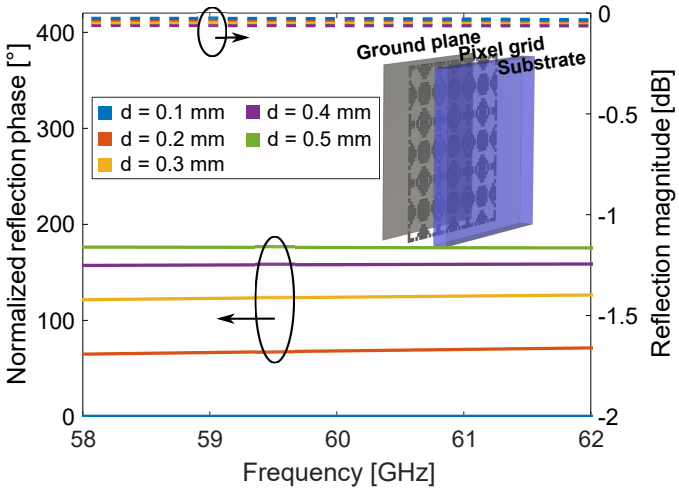

Fig. 6. Simulated performance of the selected solution. Normalized phased (solid lines) and magnitude (dashed lines) of the reflected wave for different ground plane displacements.

The phase and magnitude responses depicted in Fig. 6 confirm the good performance of the optimized design. A flat phase response with a less than 4° divergence from the targeted phase shift value of 180° is obtained for the maximum displacement of the ground plane. Moreover, the losses are kept below 0.1 dB for the whole frequency band, which signifies an ultra-low loss response of the device. Similarly, this level of losses is considerably below the established loss threshold for the penalization coefficient α_l, which was set to l_t = 0.5 dB. This means that, for the selected solution, the value of the coefficient is zero, canceling its effect. This phenomenon

is mainly due to the absence of abrupt resonances inside the operating frequency range, which is already favored by the objective function q_{lin}. In fact, avoiding deep resonances is key to achieving a perfectly linear response, since they would cause an isolated fluctuation of the phase, and hence a deviation from the targeted ideal function. However, in other possible scenarios, in which the losses penalization coefficient α_l would be applied to more complex objectives such as non-linear phase distribution profiles or wide-angle response, it would have a more determinant role, preserving the low-loss response of the device while optimizing for the rest of objectives.

Despite not being the best solution in terms of linearity from the ones obtained after optimization (the maximum phase error criterion was applied to restrict the selectable range of solutions among the ones displayed in Fig. 5), the structure presents a quite linear response, enough to precisely control the phase with the help of a piezoelectric actuator (see Fig. 11 for a better insight of the linearity of the solution).

In the following, a prototype is fabricated based on the selected solution from optimization, and its performance is measured in a broadband frequency range.

IV. Prototype Fabrication and Characterization

In this section, details regarding the fabrication and characterization processes of the proposed prototypes are presented.

A. Fabrication details

The fabricated periodic array is depicted in Fig. 7. It consists of an array of four elements as produced and chosen by the aforementioned optimization approach.

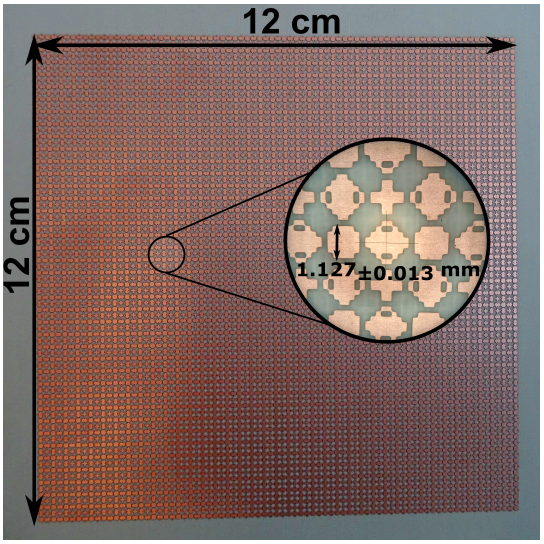

Fig. 7. Fabricated metallic metasurface deposited on the dielectric and microscopic details of a few unit cells.

The overall dimensions of the squared board are 12x12 cm. Standard PCB methods were sourced to fabricate the pixel grid structure, using NY9220ST0787S1S1 and NY9220ST0787N1N1 AGC substrate material with dielectric constant ε_r = 2.2 and thickness w = 0.78 mm, with a loss tangent of 0.0009.

In order to make an analysis of the exactitude of the fabrication, the dimensions of some components of the unit cell were analyzed with the help of a microscope. After measuring the side of the pseudo-square component of several unit cells (see detail in Fig. 7) spread along the structure, a standard variation of approximately 0.013 mm was observed, which leads to a fabrication tolerance of around 13 microns. Moreover, the average value of this dimension (the side contains a total of 6 pixels) was 1.127 mm, which is very close to the design value used in the simulation ($p_w \cdot \#pixels = 0.1875 \cdot 6 = 1.125$ mm).

B. Characterization setup and instrumentation

The setup of the experiment for the characterization of the device is the one included in Fig. 8, which corresponds with the EM influence area as previously defined in Fig. 2. Two standard gain horn antennas WR15 by Flann Microwave are placed in front of the device at a distance that ensures the far-field condition. Then, the prototype is properly fixed between the two white lateral panels and aligned with the ground plane. A ZVA 67A (Rohde & Schwarz) Vector Network Analyzer (VNA) is used to sweep the appropriate frequency ranges. Specialized phase stable cables (ZV.796) were used to ensure accurate reporting of phase measurements. The transmission coefficient between both antennas is then read from the VNA and interpreted as the reflection coefficient (Γ) of the system. A single antenna could also be used for the characterization, but this would lead to the appearance of standing wave effects, creating ripples and interference in the results.

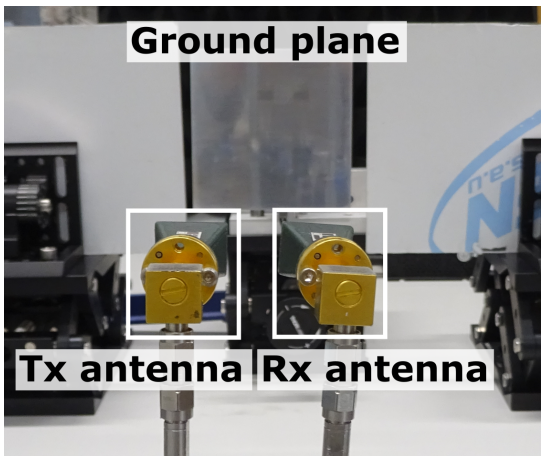

Fig. 8. Transmitting and receiving antennas pointing to the ground plane (EM influence zone).

In order to extract measured Γ, the following expression is employed to get rid of the influence of the environment and obtain accurate magnitude results by using the cases of the ground plane and free space as references:

$$\Gamma = \frac{\Gamma_{metasurface} - \Gamma_{freeSpace}}{\Gamma_{freeSpace} - \Gamma_{groundPlane}} \tag{6}$$

where $\Gamma_{metasurface}$, $\Gamma_{groundPlane}$, $\Gamma_{freeSpace}$ correspond to the transmission coefficients from one antenna to the other

when the metasurface, just the metallic ground plane, and the air is used as the sample, respectively. Also, it is worth mentioning that time-domain filtering is applied to the characterization results. With this, we ensure that the processed signal is exempt from the impact of possible multi-path reflections or any other undesired signal different from the one reflected by the device.

The elements conforming the reconfiguration engine i.e. the electro-mechanical system that allows for the displacement of the ground plane, are depicted in Fig. 9.

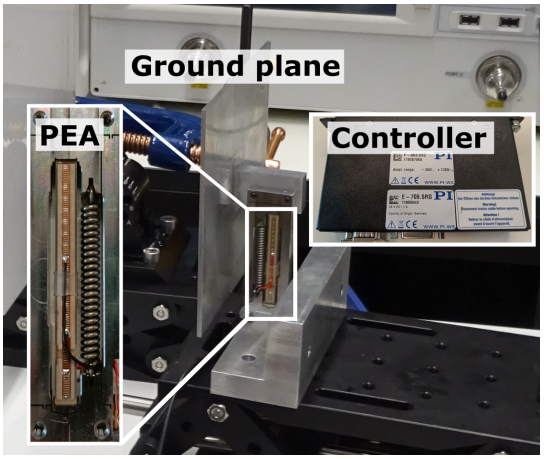

Fig. 9. Reconfiguration system (piezo-electric actuator, controller, and moving ground plane).

The employed piezo-electric actuator is the PiezoMove P-603.5S1 (by Physik Instrumente Ltd UK) with dimensions of 62x21 mm. Numerous thin disks of piezo-electric material Lead (Pb) Zirconate (Zr) Titanate (Ti) (PZT) are stacked on top of each other and biased via interleaved electrodes. Due to the inverse piezo-electric effect each of the disks has the ability to expand vertically when exposed to voltage. The above-mentioned configuration is packaged inside an arrangement of flexures providing precision guidance and amplified motion. The maximum travel distance achieved by the proposed piezo-electric actuator is 0.50 mm, with nanometer accuracy. This displacement is more than enough to design reconfigurable structures at millimeter wave frequencies. In addition, this mechanism can be used up to low THz frequencies. The flexure PEA speed is typically in the order of milliseconds and varies depending on load. The ground plane designed for this experiment is made of aluminum, weighing 70 grams. Based on the weight of the ground plane, a switching speed of less than two milliseconds could be expected. To control the aforementioned commercial PEA we used a dedicated controller E-709.SRG from the same company. This controller has a strain gauge sensor and can provide the position with respect to an initial reference point. The linear movement of the actuator controlled by the controller has a maximum error of 0.02 %. The main advantage of utilizing such a controller (which is manipulated thanks to a software interface installed in a computer) is that it allows the user to introduce the desired ground plane displacement into the interface directly. Then, the controller would transform this displacement value into the correspondent needed driven voltage for the actuator, which ranges between -20 and 200 V.

V. Results and Discussion

The results obtained from the characterization of the fabricated prototype are presented below, together with an electromagnetic analysis of the broadband response of the device.

A. Experimental results

Fig. 10 includes the obtained magnitude and normalized phase shift for both simulation and experimentation results.

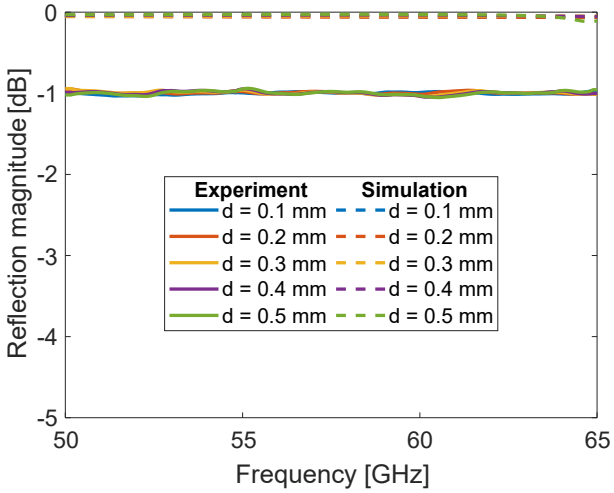

(a) Reflection amplitude.

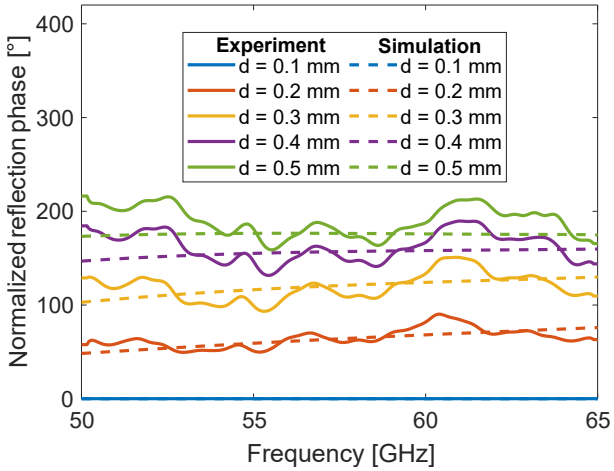

(b) Normalized reflection phase.

Fig. 10. Simulated and experimental results between 50 and 65 GHz for different displacements of the ground plane.

Despite the optimization phase being conducted considering an operating band between 58 and 62 GHz, the structure has been tested for a wider frequency range, showing a considerably good performance from 50 to 65 GHz. Also, it is worth mentioning that all experiments have been conducted for the case of normal incidence ($\theta = 0°$), although small variations from the ideal scenario might occur due to the fact that the two antennas cannot be positioned completely parallel to each other (see setup in Fig. 8).

As it can be observed in Fig. 10a, a considerably constant level of 1 dB losses is obtained for all the different positions of the ground plane. This signifies around 1 dB difference w.r.t. the simulation results (in which losses are below 0.01 dB for the whole band). This mismatch is logical when taking into account the number of factors affecting the magnitude at these frequencies. Moreover, the value of the loss tangent employed for the dielectric in simulation is based on the specifications of the material provider, which are given for a frequency of 10 GHz. According to a classical dispersive profile of such a material, this value might be higher around 60 GHz, resulting in an augmentation of the losses, hence leading to a better agreement with the experimental result. Nonetheless, this result confirms the ultra-loss character of the structure and outperforms the performance of similar structures recently published in the literature, as showcased below in Table I.

Regarding the phase shift, despite the slight phase fluctuations at some frequencies, the experimental results confirm the expected behavior of the device. A progressive and linear evolution of the phase between 0 and 180° is achieved by varying the ground plane distance from up to 0.5 mm. This is maintained for the whole frequency range between 50 and 65 GHz, translating into a fractional bandwidth of 26%.

Some considerations should be made about the nature of the surface of the fabricated board and its impact on the empirical distance between the structure and the ground plane.

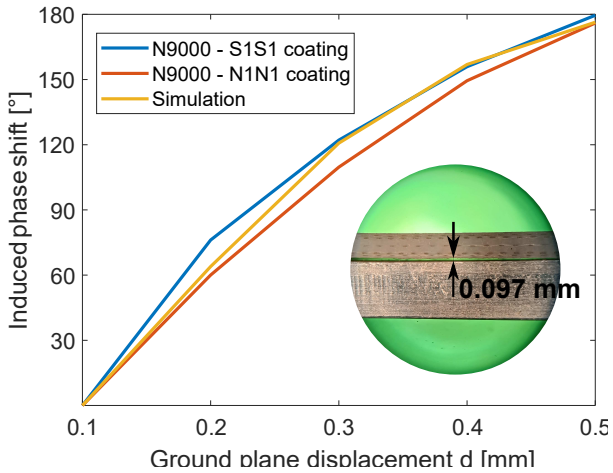

Fig. 11. Induced phase shift w.r.t ground plane displacement at center frequency (57.5 GHz). Experimental results of the two fabricated prototypes vs simulation and microscope illustration of the structure touching the ground plane.

This is illustrated in the microscope image included in Fig. 11, where a microcavity of almost 0.1 mm has been created between the board and the metallic plane, despite of the fact that the structure was touching the ground plane. These microcavities are irregular along the whole surface of the board and can vary from a few microns up to 100 microns.

According to this, when a certain value of d is considered for the experimental measurements, the real distance from the structure to the ground plane will vary irregularly by ± 0.1 mm due to the microcavities. The latter could explain the slight phase fluctuations of the experimental results at some frequencies observed in Fig. 10b. Since the possible existence of these microcavities was known by the authors prior to fabrication, this is the reason why the minimum distance considered for simulation is d_{min} = 0.1 mm.

Considering this, the curves of the Fig. 11 can be now interpreted. The linearity of the response and the good agreement with the simulation confirm the satisfactory performance of the prototype. Moreover, two fabricated prototypes with different metal coatings (preserving an identical metasurface design) are compared. Although they contain the same dielectric material, some roughness differences can be noted in the material coatings. This is illustrated in the microscopic images of Fig. 12.

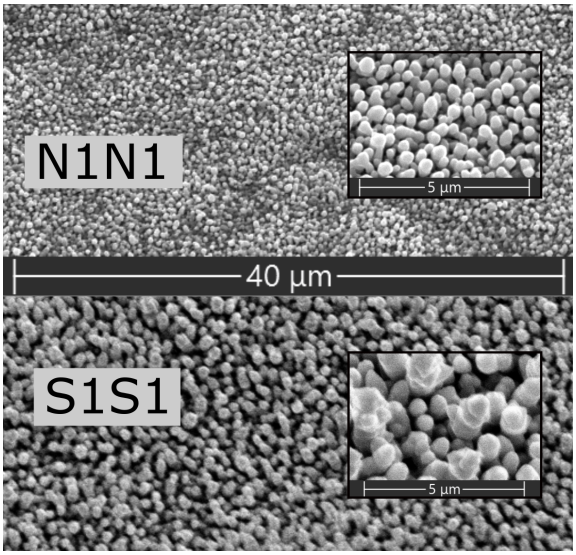

Fig. 12. Microscopic images of the two different metal coatings.

The fact that both materials provided almost identical results increases the degrees of freedom when it comes to the selection of the substrate material, which can reduce the fabrication cost in many cases. Note that the losses of both prototypes are also very similar, and no magnitude comparison of both structures is included in the manuscript to avoid redundancy with Fig. 10a.

Ref.	Unit cell geometry	Technology	f (GHz) FBW	Loss (dB)	Lin.
[28]	Microstrip patches	Liquid crystal	76-78 2.6%	6.7	✗
[29]	Four-legged loaded elements	MEMS	28.6-31.8 10.6%	2	✗
[30]	Microstrip patches	PIN diodes	59.7-62.5 4.6%	4.5	✗
[17]	Squared and cross resonators	PEA	50-65 26%	∼2	✗
This work	256-elements pixel grid	PEA	50-65 26%	1.05	✓

TABLE I
COMPARISON OF DIFFERENT STATE-OF-THE-ART RECONFIGURABLE METASURFACE-BASED PHASE SHIFTERS

Table I includes a comparison of various reconfigurable phase shifters existing in the literature. They are contrasted in terms of their unit cell geometry, the method used to achieve dynamic phase shift (technology), and their performance in terms of bandwidth, losses, and linearity.

Most of the unit cell geometries are composed of well-known resonator shapes (split-ring, square, cross-shaped...). Regarding the reconfiguration technology, the majority of the existing designs use active methods, which offer their best performance at lower frequency bands, becoming considerably lossy at high mm-wave frequencies. Moreover, the utilization of such components (diodes, liquid crystal...) requires complex circuitry, which can become bulky at high frequencies. In this work, an unprecedented value of losses below 1 dB has been achieved for a fractional bandwidth of 26% around 60 GHz. Moreover, going one step further from the designs presented in [17], an innovative and non-intuitive unit cell geometry is obtained through optimization, considering the linearity of the phase response as an objective through the design process.

B. Broadband electromagnetic analysis

Fig. 13 illustrates the surface current distribution at the lowest and highest frequencies for the minimum and maximum positions of the ground plane.

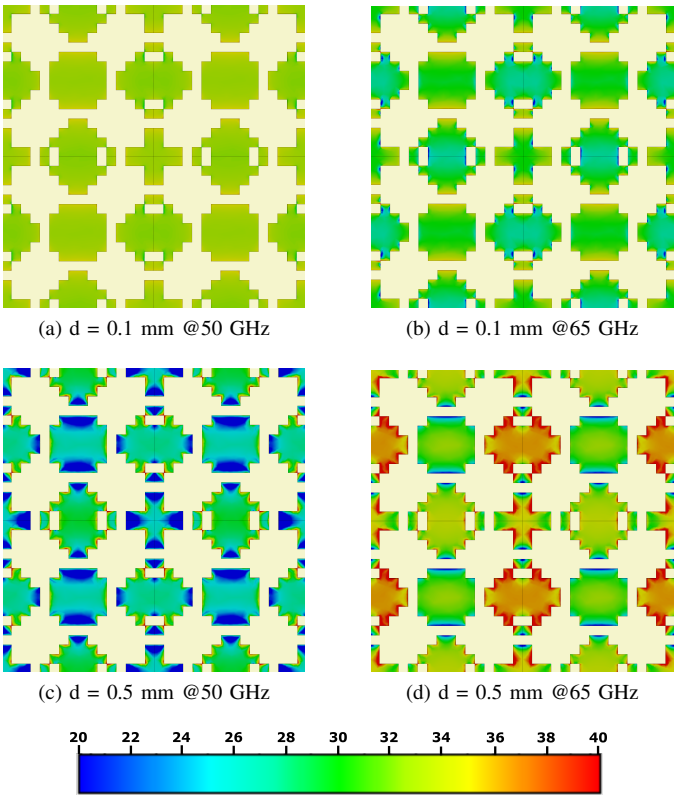

(a) d = 0.1 mm @50 GHz (b) d = 0.1 mm @65 GHz

(c) d = 0.5 mm @50 GHz (d) d = 0.5 mm @65 GHz

Fig. 13. Surface current distribution on the pixel grid of the metasurface for different frequencies and ground plane displacements. Units are in dB(A/m).

According to the current distribution, some conclusions can be extracted to better understand the broadband behavior of the device. First, it can be observed how the current is weaker when the ground plane is closer to the structure (Figs. 13a and 13b). In this position, most of the current is located on the surface of the ground plane rather than on the pixel grid. On the contrary, when the ground plane gets further from the structure, the surface current on the pixel grid increases considerably, as depicted in Figs. 13c and 13d. Secondly, it is worth remarking that the current tends to be more uniform and expanded along the whole pixel surface at lower frequencies, whereas it is rather concentrated on the edges and corners (thus, elements with smaller sizes) at higher frequencies. This phenomenon is a direct consequence of the variation of the wavelength and gives some insights into the mechanisms that allow the structure to adapt well along such a wide frequency range.

VI. Conclusions

A dynamic metasurface phase shifter at mm-wave frequencies has been proposed and validated. The design is obtained through an innovative methodology that uses multi-objective optimization to obtain a unit-cell design providing ultra-low losses and a linear response. Two prototypes are fabricated and characterized, performing an analysis on dielectric materials with different metal coating for the substrate. The results show a satisfactory phase-shifting performance from 50 to 65 GHz. Moreover, the loss level is kept around 1 dB for the whole frequency range, and a linear response is shown for the induced phase shift w.r.t. the displacement of the ground plane. Finally, an electromagnetic analysis has been performed, revealing some of the physical phenomena that enable the wide-band performance of the device. Future works could focus on the integration of this structure in a complete mm-wave antenna system.

Acknowledgment

The authors would like to thank AGC Multi Material Europe for providing us with the NY9220ST0787S1S1 and NY9220ST0787N1N1 Nelco substrates.

References

[1] P. Nayeri, F. Yang, and A. Z. Elsherbeni, "Beam-scanning reflectarray antennas: A technical overview and state of the art," *IEEE Antennas Propag Mag*, vol. 57, pp. 32–47, 8 2015.

[2] C. Pfeiffer and A. Grbic, "Millimeter-wave transmitarrays for wavefront and polarization control," *IEEE Trans Microw Theory Tech*, vol. 61, pp. 4407–4417, 12 2013.

[3] P. H. Z. Cano, Z. D. Zaharis, T. V. Yioultsis, N. V. Kantartzis, and P. I. Lazaridis, "Pattern reconfigurable antennas at millimeter-wave frequencies: A comprehensive survey," *IEEE Access*, 2022.

[4] M. A. Kats, D. Sharma, J. Lin, P. Genevet, R. Blanchard, Z. Yang, M. M. Qazilbash, D. N. Basov, S. Ramanathan, and F. Capasso, "Ultra-thin perfect absorber employing a tunable phase change material," *Appl. Phys. Lett.*, vol. 101, 11 2012.

[5] S. Sun, Q. He, S. Xiao, Q. Xu, X. Li, and L. Zhou, "Gradient-index meta-surfaces as a bridge linking propagating waves and surface waves," *Nat. Mater.*, vol. 11, pp. 426–431, 2012.

[6] J. Xu, R. Li, S. Wang, and T. Han, "Ultra-broadband linear polarization converter based on anisotropic metasurface," *Opt. Express*, vol. 26, p. 26235, 10 2018.

[7] J. White, "Diode phase shifters for array antennas," *IEEE Trans Microw Theory Tech*, vol. 22, pp. 658–674, 1974.

[8] L. Whicker, "Review of ferrite phase shifter technology," *1973 IEEE G-MTT International Microwave Symposium*, pp. 95–97, 1973.

[9] Z. Qamar, S. Y. Zheng, W. S. Chan, and D. Ho, "An equal-length multiway differential metamaterial phase shifter," *IEEE Trans Microw Theory Tech*, vol. 65, pp. 136–146, 1 2017.
[10] J. H. Park, H. T. Kim, W. Choi, Y. Kwon, and Y. K. Kim, "V-band reflection-type phase shifters using micromachined CPW coupler and RF switches," *J Microelectromech Syst.*, vol. 11, pp. 808–814, 12 2002.
[11] X. G. Luo, "Principles of electromagnetic waves in metasurfaces," *Science China: Physics, Mechanics and Astronomy*, vol. 58, 9 2015.
[12] F. Falcone, T. Lopetegi, M. A. Laso, J. D. Baena, J. Bonache, M. Beruete, R. Marques, F. Martín, and M. Sorolla, "Babinet principle applied to the design of metasurfaces and metamaterials," *Phys. Rev. Lett.*, vol. 93, 11 2004.
[13] H. Li, Y. B. Li, C. Y. Gong, S. Y. Dong, S. Y. Wang, H. P. Wang, and T. J. Cui, "Design of programmable transmitarray antenna with independent controls of transmission amplitude and phase," *IEEE Trans. Antennas Propag.*, vol. 70, pp. 8086–8099, 9 2022.
[14] M. A. B. Abbasi, M. A. Antoniades, and S. Nikolaou, "A compact reconfigurable NRI-TL metamaterial phase shifter for antenna applications," *IEEE Trans. Antennas Propag.*, vol. 66, pp. 1025–1030, 2 2018.
[15] C. Ding, Y. J. Guo, P. Y. Qin, and Y. Yang, "A compact microstrip phase shifter employing reconfigurable defected microstrip structure (RDMS) for phased array antennas," *IEEE Trans. Antennas Propag.*, vol. 63, pp. 1985–1996, 5 2015.
[16] M. Mavridou, A. P. Feresidis, P. Gardner, and P. S. Hall, "Tunable millimetre-wave phase shifting surfaces using piezoelectric actuators," *IET Microw.*, vol. 8, pp. 829–834, 2014.
[17] E. Vassos, J. Churm, and A. Feresidis, "Ultra-low-loss tunable piezoelectric-actuated metasurfaces achieving 360° or 180° dynamic phase shift at millimeter-waves," *Scientific Reports*, vol. 10, 12 2020.
[18] M. Kovaleva, D. Bulger, and K. P. Esselle, "Cross-entropy method for design and optimization of pixelated metasurfaces," *IEEE Access*, vol. 8, pp. 224 922–224 931, 2020.
[19] D. W. Boeringer and D. H. Werner, "Particle swarm optimization versus genetic algorithms for phased array synthesis," *IEEE Trans. Antennas Propag.*, vol. 52, pp. 771–779, 3 2004.
[20] J. H. Barton, C. R. Garcia, E. A. Berry, R. Salas, and R. C. Rumpf, "3-D printed all-dielectric frequency selective surface with large bandwidth and field of view," *IEEE Trans. Antennas Propag.*, vol. 63, pp. 1032–1039, 2015.
[21] Z. Zhou, K. Chen, B. Zhu, J. Zhao, Y. Feng, and Y. Li, "Ultra-wideband microwave absorption by design and optimization of metasurface salisbury screen," *IEEE Access*, vol. 6, pp. 26 843–26 853, 5 2018.
[22] P. H. Z. Cano, E. Vassos, Z. D. Zaharis, P. Lazaridis, T. V. Yioultsis, N. V. Kantartzis, and A. Feresidis, "Optimization-driven design of a 90° metasurface phase shifter at 60 GHz," in *2022 IEEE International Black Sea Conference on Communications and Networking (BlackSeaCom)*, 2022, pp. 26–29.
[23] "CST Studio Suite. [online]. Available: https://www.3ds.com."
[24] A. Benítez-Hidalgo, A. J. Nebro, J. García-Nieto, I. Oregi, and J. D. Ser, "jMetalPy: A Python framework for multi-objective optimization with metaheuristics," *Swarm Evol. Comput.*, vol. 51, 12 2019.
[25] K. Deb, A. Pratap, S. Agarwal, and T. Meyarivan, "A fast and elitist multiobjective genetic algorithm: NSGA-II," *IEEE Trans. Evol. Comput.*, vol. 6, pp. 182–197, 2002.
[26] A. J. Nebro, J. Galeano-Brajones, F. Luna, and C. A. C. Coello, "Is NSGA-II ready for large-scale multi-objective optimization?" *Math. Comput. Appl.*, vol. 27, p. 103, 11 2022. [Online]. Available: https://www.mdpi.com/2297-8747/27/6/103
[27] W. Roh, J.-Y. Seol, J. Park, B. Lee, J. Lee, Y. Kim, J. Cho, and K. Cheun, "Millimeter-wave beamforming as an enabling technology for 5G cellular communications: Theoretical feasibility and prototype," *IEEE Commun. Mag.*, vol. 52, pp. 106–113, 2 2014.
[28] A. Moessinger, R. Marin, J. Freese, S. Mueller, A. Manabe, and R. Jakoby, "Investigations on 77 GHz tunable reflectarray unit cells with liquid crystal," *European Space Agency, (Special Publication) ESA SP*, vol. 626 SP, 2006.
[29] B. Schoenlinner, A. Abbaspour-Tamijani, L. C. Kempel, and G. M. Rebeiz, "Switchable low-loss RF MEMS Ka-band frequency-selective surface," *IEEE Trans Microw Theory Tech*, vol. 52, pp. 2474–2481, 11 2004.
[30] H. Kamoda, T. Iwasaki, J. Tsumochi, and T. Kuki, "60-GHz electrically reconfigurable reflectarray using p-i-n diode," *IEEE MTT-S Int. Microw.*, pp. 1177–1180, 2009.

Pablo H. Zapata Cano (S'22) received the B.Sc. degree in Telecommunications Engineering from the University of Granada in 2018. In 2021, he received the M.Sc. degrees in Photonic Systems and Optical Networks from Télécom SudParis and in Informatics and Telecommunications from the National and Kapodistrian University of Athens, under the SMARTNET Erasmus Mundus Joint Master Degree (EMJMD) program. Since 2018, he has been an active researcher with the affiliations of University of Granada, University of Málaga and Thales Research and Technology. Currently, he is a PhD candidate at the Aristotle University of Thessaloniki, were he is a recipient of a Marie Curie H2020 scholarship. His research interests include reconfigurable devices, millimeter-wave antennas, computational physics, engineered materials and optimization.

Evangelos Vassos Evangelos Vassos was born in Thessaloniki, Greece, in 1993. He received his B.Sc. degree (Ptychio) in Physics from Aristotle University of Thessaloniki (AUTH), Greece, in 2015, followed by an M.Sc. degree in Telecommunications Engineering (radioelectrology) from the same institution in 2017. He earned his Ph.D. in the Department of Electronic, Electrical and Systems Engineering at the University of Birmingham (UoB), UK, in 2022. As part of a Defence Science and Technology Laboratory (DSTL) funded program in 2020, Evangelos developed electro-optical emissivity control metasurfaces. He also worked as a research fellow in the second half of 2021 on the EPSRC-funded SYMETA program, investigating 3D-printed isotropic and anisotropic artificial dielectrics for antennas and RF devices. Currently, Evangelos is working on the ANISAT project, an EPSRC-funded scheme that focuses on anisotropic microwave/terahertz metamaterials for satellite applications. His research interests lie in the fields of microwave/millimetre/terahertz/infrared metamaterials and metasurfaces, tuning technologies, and reflectarray antennas for telecommunications and satellite applications.

Zaharias D. Zaharis (M'13–SM'15) received the B.Sc. degree in physics, the M.Sc. degree in electronics, the Ph.D. degree in antennas and propagation modeling for mobile communications, and the Diploma degree in electrical and computer engineering from the Aristotle University of Thessaloniki, Thessaloniki, Greece, in 1987, 1994, 2000, and 2011, respectively. From 2002 to 2013, he was with the Administration of the Telecommunications Network of the Aristotle University of Thessaloniki. Since 2013, he has been with the School of Electrical and Computer Engineering of the Aristotle University of Thessaloniki. He has been involved in several international research projects, such as EU Horizon 2020 MOTOR5G and RECOMBINE. He is the author of 81 scientific journal papers, 77 international conference papers, 5 book chapters, and one textbook. Recently, he was elected Chair of the Electron Devices / Microwave Theory and Techniques / Antennas and Propagation Joint Chapter of the IEEE Greece Section. His current research interests include design and optimization of antennas and microwave circuits, signal processing on smart antennas, development of evolutionary optimization algorithms, and neural networks. Dr. Zaharis is a member of the Technical Chamber of Greece, and is currently serving as an Associate Editor for IEEE ACCESS.

Pavlos I. Lazaridis (M'13–SM'15) received the Diploma degree in electrical engineering from the Aristotle University of Thessaloniki, Thessaloniki, Greece, in 1990, the M.Sc. degree in electronics from Université Pierre and Marie Curie (Paris 6), Paris, France, in 1992, and the Ph.D. degree from the École Nationale Supérieure des Télécommunications (ENST) Paris and Université Paris 6, in 1996. From 1991 to 1996, he was involved in research at France Télécom, and teaching at ENST Paris. In 1997, he became the Head of the Antennas and Propagation Laboratory, Télédiffusion de France/the France Télécom Research Center (TDF–C2R Metz). From 1998 to 2002, he was a Senior Examiner with the European Patent Office (EPO), The Hague, The Netherlands. From 2002 to 2014, he was involved in teaching and research with the ATEI of Thessaloniki, Thessaloniki, Greece, and Brunel University, London, U.K. He is currently a Professor of electronics and telecommunications with the University of Huddersfield, U.K. He has been involved in several international research projects, such as EU Horizon 2020 MOTOR5G and RECOMBINE, NATO-SfP ORCA, and he has published over 200 research articles and several national and European patents. He is a member of the IET (MIET), Senior Member of URSI, and a Fellow of the Higher Education Academy (FHEA). He is currently serving as an Associate Editor for IEEE Access.

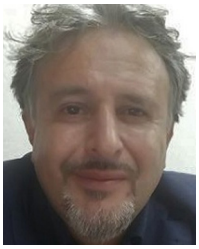

Traianos V. Yioultsis (M'09) received the Diploma and Ph.D. degrees in electrical and computer engineering from the Aristotle University of Thessaloniki, Thessaloniki, Greece, in 1992 and 1998, respectively. From 2001 to 2002, he was a Post-Doctoral Research Associate with the Department of Electrical and Computer Engineering, University of Illinois at Urbana–Champaign, Champaign, IL, USA. Since 2002, he has been with the Department of Electrical and Computer Engineering, Aristotle University of Thessaloniki, where he is currently a Professor. His current interests include the analysis and design of antennas and microwave circuits with fast computational techniques, and the modeling of complex wave propagation problems. Dr. Yioultsis has served as a member of the Editorial Board for IEEE Communications Letters and several international conferences.

Nikolaos V. Kantartzis (M'99–SM'12) received the Diploma and Ph.D. degrees in Electrical and Computer Engineering from the Aristotle University of Thessaloniki, Thessaloniki, Greece, in 1994 and 1999, respectively. In 1999, he joined the Applied and Computational Electromagnetics Laboratory of the same department, where he is currently a Professor. He coauthored Higher-Order FDTD Schemes for Waveguide and Antenna Structures (Morgan & Claypool Publishers: San Rafael, CA, 2006) and Modern EMC Analysis Techniques I & II (Morgan & Claypool Publishers: San Rafael, CA, 2008). Moreover, he has authored or coauthored more than 175 peer-reviewed journal papers and more than 270 publications in international conference proceedings. His main research interests include computational electromagnetics, EMC modeling, metamaterials/metasurfaces, graphene, and microwave structures,. Dr. Kantartzis is a Senior Member of IEEE and the recipient of several scholarships, distinctions, and awards, such as the 1999 URSI General Assembly Young Scientist Award, the 2002 COMPEL Most Outstanding Paper Award of Excellence, the EMC Europe 2004 Best Paper Award, the 2013 Metamaterials 3rd Prize Best Paper Award, the 2014 Computation in Electromagnetics Conference Best Paper Award, and the 2014 SPIE Photonics Europe Best Paper Award (Metamaterials Section).

Alexandros P. Feresidis (S'98-M'01-SM'08) was born in Thessaloniki, Greece, in 1975. He received the Physics degree from Aristotle University of Thessaloniki, Greece, in 1997, and the MSc(Eng) in Radio Communications and High Frequency Engineering from the University of Leeds, UK, in 1998. In 2002, he obtained the Ph.D. in Electronic and Electrical Engineering from Loughborough University, UK. During the first half of 2002, he was a research associate and in the same year he was appointed Lecturer in Wireless Communications in the Department of Electronic and Electrical Engineering, Loughborough University, UK, where, in 2006, he was promoted to Senior Lecturer. In December 2011 he joined the Department of Electronic, Electrical and Systems Engineering, University of Birmingham, UK, where he is currently a Professor of Microwave and Terahertz Communications. He has published more than 190 papers in peer reviewed international journals and conference proceedings and has co-authored five book chapters. His research interests include analysis and design of metamaterials, electromagnetic band gap (EBG) structures and frequency selective surfaces (FSS), leaky-wave antennas, small/compact antennas, passive microwave/mm-wave/THz circuits, microfabrication, numerical techniques for electromagnetics and bioelectromagnetics. Dr Feresidis has held a Senior Research Fellowship Award from the U.K. Royal Academy of Engineering and The Leverhulme Trust (2013-2014). He is a member of the UK EPSRC Peer Review College, he was on the editorial board of IET Microwaves, Antennas and Propagation journal (2014-2018) and he is currently an Associate Editor in the IEEE Transactions on Antennas and Propagation.